Science Advances

AAAS

advances.sciencemag.org/cgi/content/full/3/9/e1701377/DC1

Supplementary Materials for

Electrical access to critical coupling of circularly polarized waves in graphene chiral metamaterials

Teun-Teun Kim, Sang Soon Oh, Hyeon-Don Kim, Hyun Sung Park, Ortwin Hess, Bumki Min, Shuang Zhang

Published 29 September 2017, *Sci. Adv.* **3**, e1701377 (2017)
DOI: 10.1126/sciadv.1701377

This PDF file includes:

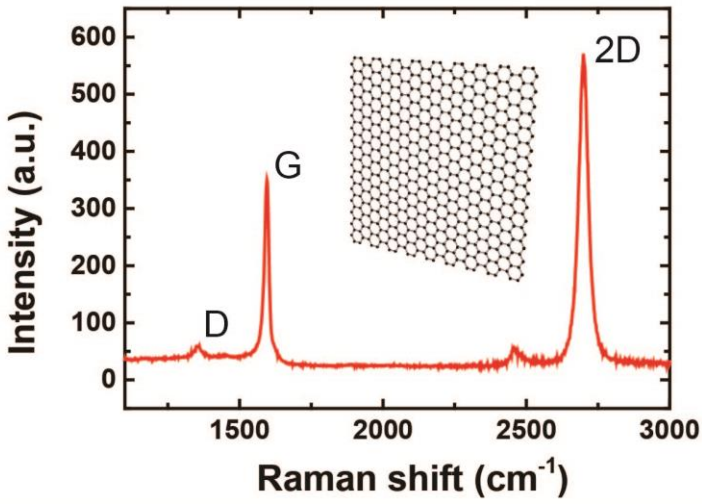

fig. S1. Characterization of single-layer graphene by Raman spectroscopy. CVD-grown graphene layer used for the device fabrication is characterized by Raman spectroscopy. The representative signatures of single-layer graphene can be observed (46). The intensity ratio of the 2D and G peaks (I_{2D} / I_G) is higher than 1.6. The D, G and 2D peaks were located at ~1355, 1595, and 2699 cm^{-1}, respectively. The full width at half maximum (FWHZ) of the 2D-peak is 38 cm^{-1}. Raman spectroscopic measurements confirmed the presence of monolayer graphene when averaged over the whole area of the wafer. During the synthesis and fabrication processes, CVD-grown graphene easily becomes *p*-doped (41), which was also the case for our graphene samples.

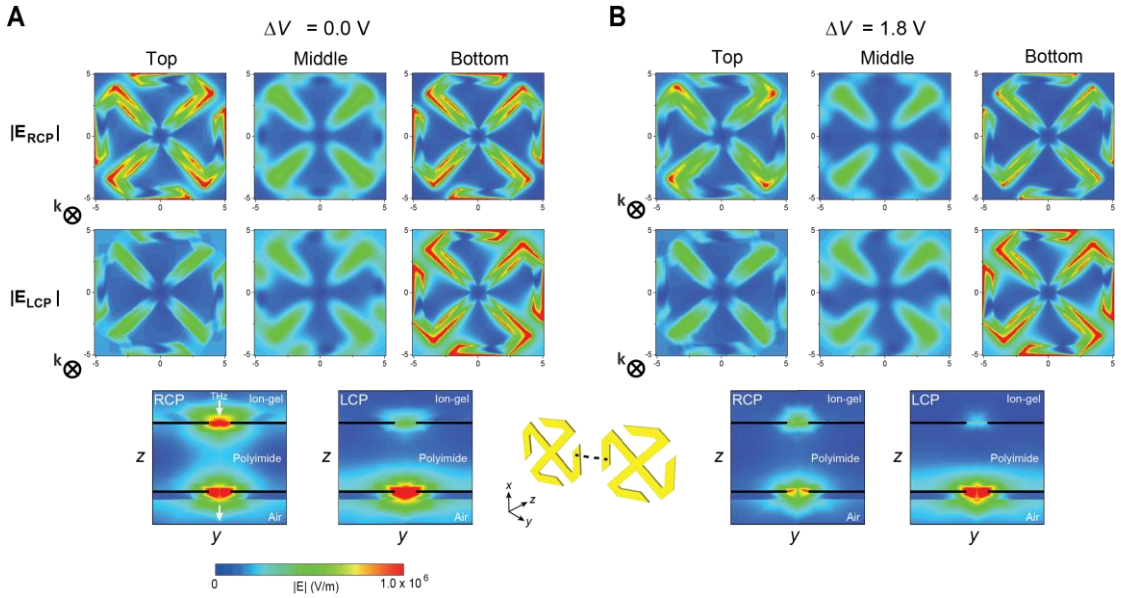

fig. S2. Electric field distribution. Electric field distribution for RCP ($|\mathbf{E}_{LCP}|$) and LCP ($|\mathbf{E}_{RCP}|$) in the CDZM with gate voltage ΔV equal to (**A**) 0 V and (**B**) 1.8 V at the frequency 1.1 THz. In the case of ΔV = 0.0 V, electric fields corresponding to the RCP incident wave are confined mostly in the dielectric substrates between the top and bottom metal strips of the central and side arms of the CDZM as well as in the gap between adjacent CDZMs; however, for the LCP wave, the electric fields are mainly confined in that of bottom. This difference in the field distribution results in difference in transmittance for RCP and LCP waves. By increasing ΔV to 1.8 V, the graphene layer becomes more conductive, by which the field enhancement at the top surface of the CDZM is reduced for RCP polarization. On the other hand, the field distribution for the LCP wave is not affected much by the increase of ΔV for the RCP as the field strength near the top surface of CDZM is low for LCP polarization.

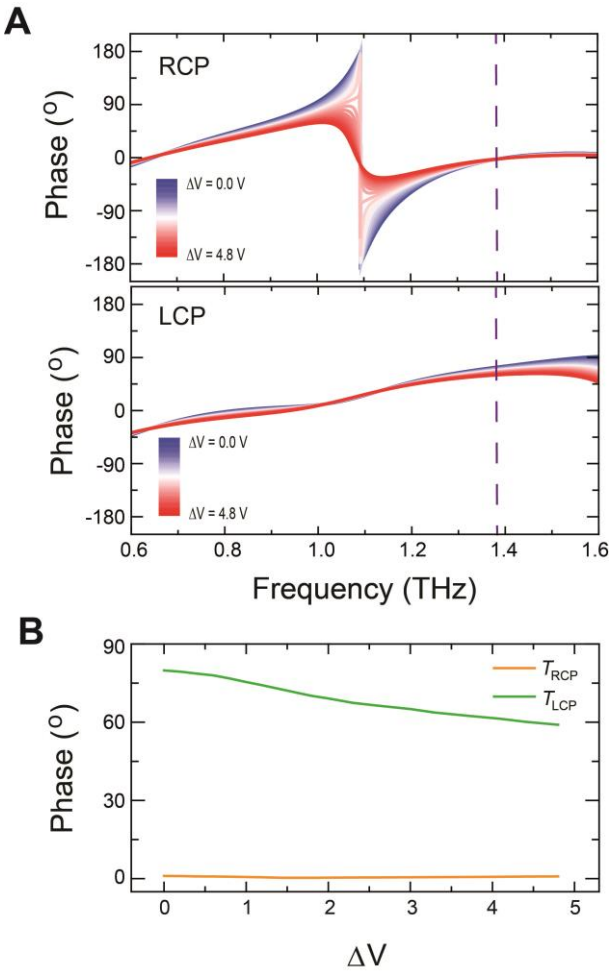

fig. S3. Transmission phase spectra. (**A**) Simulated transmission phase spectra for RCP and LCP in the CDZM with gate voltage ΔV. (**B**) Transmission phase spectra for RCP (orange) and LCP (green) at the frequency ellipticity $\eta \approx 0$ as a function of ΔV.

note S1. Temporal CMT for two ports and two resonances.

To calculate the scattering matrix for our chiral metamaterial, we applied the temporal coupled-mode theory by S. Fan (44) to the case of two uncoupled resonances. The schematic of our model is shown in Fig. 1 in the main text. This extended model can be applied to one polarization state of either linear or circular polarizations when there is no coupling between the two polarizations. Here, we adopt Dirac's bracket notation and use the same alphabetical characters for coefficients and parameters as in the Ref. (44).

To begin with, the dynamic equations for the amplitude a_1 and a_2 of the two resonance modes can be written as

$$\frac{da_1}{dt} = \left(j\omega_1 - \frac{1}{\tau_1}\right) a_1 + \left(\langle\kappa_1|^*\right)|s_+\rangle \tag{S1}$$

$$\frac{da_2}{dt} = \left(j\omega_2 - \frac{1}{\tau_2}\right) a_2 + \left(\langle\kappa_2|^*\right)|s_+\rangle \tag{S2}$$

and

$$|s_-\rangle = S|s_+\rangle = C|s_+\rangle + a_1|d_1\rangle + a_2|d_2\rangle \tag{S3}$$

where $\omega_{1,2}$ and $\tau_{1,2}$ are the resonance frequencies of the two resonance modes which corresponds to $2\pi f_{1,2}$ and $2\pi/(\Gamma_{1i,2i} + \Gamma_{1r,2r})$ in the main text respectively. $|s_+\rangle$ and $|s_-\rangle$ represent the incoming and outgoing waves and $|\kappa_{1,2}\rangle$ and $|d_{1,2}\rangle$ are the coupling coefficients between resonance modes and the incoming and outgoing waves. Here, S is the scattering matrix for the whole system and C is the scattering matrix for a direct transport process. Note that there is no coupling between the two resonances, which is a valid assumption when the two resonance frequencies are far from each other.

For a two-port system, the ket states can be represented by two components matrices. Thus, the incoming/outgoing waves are

$$|s_-\rangle = \begin{pmatrix} s_{1-} \\ s_{2-} \end{pmatrix}, \quad |s_+\rangle = \begin{pmatrix} s_{1+} \\ s_{2+} \end{pmatrix} \tag{S4}$$

Similarly, the coupling coefficients are

$$|d_1\rangle = \begin{pmatrix} d_{11} \\ d_{12} \end{pmatrix}, \quad |d_2\rangle = \begin{pmatrix} d_{21} \\ d_{22} \end{pmatrix} \tag{S5}$$

and

$$|\kappa_1\rangle = \begin{pmatrix} \kappa_{11} \\ \kappa_{12} \end{pmatrix}, \quad |\kappa_2\rangle = \begin{pmatrix} \kappa_{21} \\ \kappa_{22} \end{pmatrix} \tag{S6}$$

The scattering matrix can be written using the reflection and transmission coefficients for the whole system as

$$S = \begin{pmatrix} r & jt \\ jt & r \end{pmatrix} \tag{S7}$$

If the plane wave assumption $e^{j\omega t}$ is used in the Eq. (S4), (S5), and (S6), the outgoing wave can be written as

$$|s_-\rangle = \left[C + \frac{|d_1\rangle\langle\kappa_1|^*}{j(\omega-\omega_1)+1/\tau_1} + \frac{|d_2\rangle\langle\kappa_2|^*}{j(\omega-\omega_2)+1/\tau_2}\right]|s_+\rangle \tag{S8}$$

The terms in the bracket on the right-hand side of Eq. (S8) is the scattering matrix S for the whole system. Using the Eq. (S7) and (S8), we can obtain the reflection and transmission coefficients for the whole system.

$$r = r_0 - \frac{1/\tau_1}{j(\omega-\omega_1)+1/\tau_1} - \frac{1/\tau_2}{j(\omega-\omega_2)+1/\tau_2} \tag{S9}$$

and

$$t = t_0 - \frac{1/\tau_1}{j(\omega-\omega_1)+1/\tau_1} - \frac{1/\tau_2}{j(\omega-\omega_2)+1/\tau_2} \tag{S10}$$

For the system with both intrinsic and radiation losses, the expressions can be

$$r = r_0 - \frac{\Gamma_{1r}e^{j\phi_1}}{j(f-f_1)+\Gamma_{1r}+\Gamma_{1i}} - \frac{\Gamma_2 e^{j\phi_2}}{j(f-f_2)+\Gamma_{2r}+\Gamma_{2i}} \tag{S11}$$

and

$$t = t_0 - \frac{\Gamma_{1r}e^{j\phi_1}}{j(f-f_1)+\Gamma_{1r}+\Gamma_{1i}} - \frac{\Gamma_2 e^{j\phi_2}}{j(f-f_2)+\Gamma_{2r}+\Gamma_{2i}} \tag{S12}$$

where the phases $\phi_{1,2}$ take account of the delay due to the finite thickness of the chiral metamaterials in the coupling process between the resonance modes and incoming/outgoing waves. By changing the plane wave assumption $e^{j\omega t}$ with $e^{-i\omega t}$ in Eq. (S12), we obtain Eq. (1) in the main text.

table S1. Fitting parameters of temporal CMT.

ΔV (V)	$\boldsymbol{\phi_1}$	$\boldsymbol{\phi_2}$	$\boldsymbol{\Gamma_{1r}}$	$\boldsymbol{\Gamma_{1i}}$	$\boldsymbol{\Gamma_{2r}}$	$\boldsymbol{\Gamma_{2i}}$	$\boldsymbol{f_1}$	$\boldsymbol{f_2}$	$\boldsymbol{t_0}$
0	-3.033	1.026	0.141	0.109	0.074	0.066	0.70	1.14	0.154 + 0.024i
0.9	-3.027	1.021	0.125	0.125	0.068	0.082	0.70	1.14	0.169 + 0.023i
1.8	-3.028	0.955	0.108	0.142	0.058	0.092	0.70	1.13	0.185 + 0.018i
2.7	3.116	0.868	0.103	0.147	0.058	0.102	0.68	1.12	0.186 + 0.032i
3.6	3.038	0.796	0.098	0.152	0.057	0.1082	0.67	1.11	0.191 + 0.036i
4.8	3.032	0.770	0.082	0.168	0.048	0.122	0.67	1.10	0.199 + 0.029i